New Regulators of Clathrin-Mediated Endocytosis Identified in *Saccharomyces cerevisiae* by Systematic Quantitative Fluorescence Microscopy

Kristen B. Farrell, Caitlin Grossman, and Santiago M. Di Pietro[1]
Department of Biochemistry and Molecular Biology, Colorado State University, Fort Collins, Colorado 80523-1870

ABSTRACT Despite the importance of clathrin-mediated endocytosis (CME) for cell biology, it is unclear if all components of the machinery have been discovered and many regulatory aspects remain poorly understood. Here, using *Saccharomyces cerevisiae* and a fluorescence microscopy screening approach we identify previously unknown regulatory factors of the endocytic machinery. We further studied the top scoring protein identified in the screen, Ubx3, a member of the conserved ubiquitin regulatory X (UBX) protein family. *In vivo* and *in vitro* approaches demonstrate that Ubx3 is a new coat component. Ubx3-GFP has typical endocytic coat protein dynamics with a patch lifetime of 45 ± 3 sec. Ubx3 contains a W-box that mediates physical interaction with clathrin and Ubx3-GFP patch lifetime depends on clathrin. Deletion of the *UBX3* gene caused defects in the uptake of Lucifer Yellow and the methionine transporter Mup1 demonstrating that Ubx3 is needed for efficient endocytosis. Further, the UBX domain is required both for localization and function of Ubx3 at endocytic sites. Mechanistically, Ubx3 regulates dynamics and patch lifetime of the early arriving protein Ede1 but not later arriving coat proteins or actin assembly. Conversely, Ede1 regulates the patch lifetime of Ubx3. Ubx3 likely regulates CME via the AAA-ATPase Cdc48, a ubiquitin-editing complex. Our results uncovered new components of the CME machinery that regulate this fundamental process.

KEYWORDS clathrin; endocytosis; machinery; yeast

ENDOCYTOSIS is essential for numerous cellular activities including nutrient uptake, regulation of signal transduction, and remodeling of the cell surface (Robertson *et al.* 2009; McMahon and Boucrot 2011; Reider and Wendland 2011; Weinberg and Drubin 2012; Boettner *et al.* 2012; Kirchhausen *et al.* 2014; Merrifield and Kaksonen 2014). Clathrin-mediated endocytosis (CME) is a major endocytic pathway that collects cargo into a coated pit, invaginates and pinches off a vesicle, and transports the vesicle to endosomes. This process is carried out by a complex cellular machinery involving approximately 50 proteins to date (Robertson *et al.* 2009; McMahon and Boucrot 2011; Reider and Wendland 2011; Boettner *et al.* 2012; Weinberg and Drubin 2012; Kirchhausen *et al.* 2014; Merrifield and Kaksonen 2014). CME is highly conserved throughout evolution and proceeds through a well-choreographed sequence of events where most proteins are recruited from the cytosol at specific times (Kaksonen *et al.* 2003; Kaksonen *et al.* 2005; Idrissi *et al.* 2012; Kukulski *et al.* 2012). Although the study of these proteins' functions in the biogenesis of clathrin-coated vesicles has shed light on the mechanisms of endocytosis, many regulatory aspects of CME are still poorly understood. Furthermore, additional CME machinery components may yet to be uncovered and their functions elucidated. Previous methods for identifying endocytic machinery proteins include knockout, synthetic lethality, cargo based, and drug sensitivity screenings (Burston *et al.* 2009; Carroll *et al.* 2009). These methods may miss proteins for various reasons. A visual GFP-fusion protein-based screen identifies proteins localized to endocytic sites without excess stress on the cell due to drug or protein knockout and also has the potential to identify proteins that may not portray a strong endocytic defect in the knockout strain or cannot be deleted in the cell. Thus, by screening the yeast GFP collection for proteins that localize to sites of CME, we reasoned that it would be possible to identify new components and

doi: 10.1534/genetics.115.180729
Manuscript received July 10, 2015; accepted for publication September 7, 2015; published Early Online September 10, 2015.
Supporting information is available online at www.genetics.org/lookup/suppl/doi:10.1534/genetics.115.180729/-/DC1.
[1]Corresponding author: Department of Biochemistry and Molecular Biology, 1870 Campus Delivery, Colorado State University, Fort Collins, CO 80523-1870. E-mail: santiago.dipietro@colostate.edu

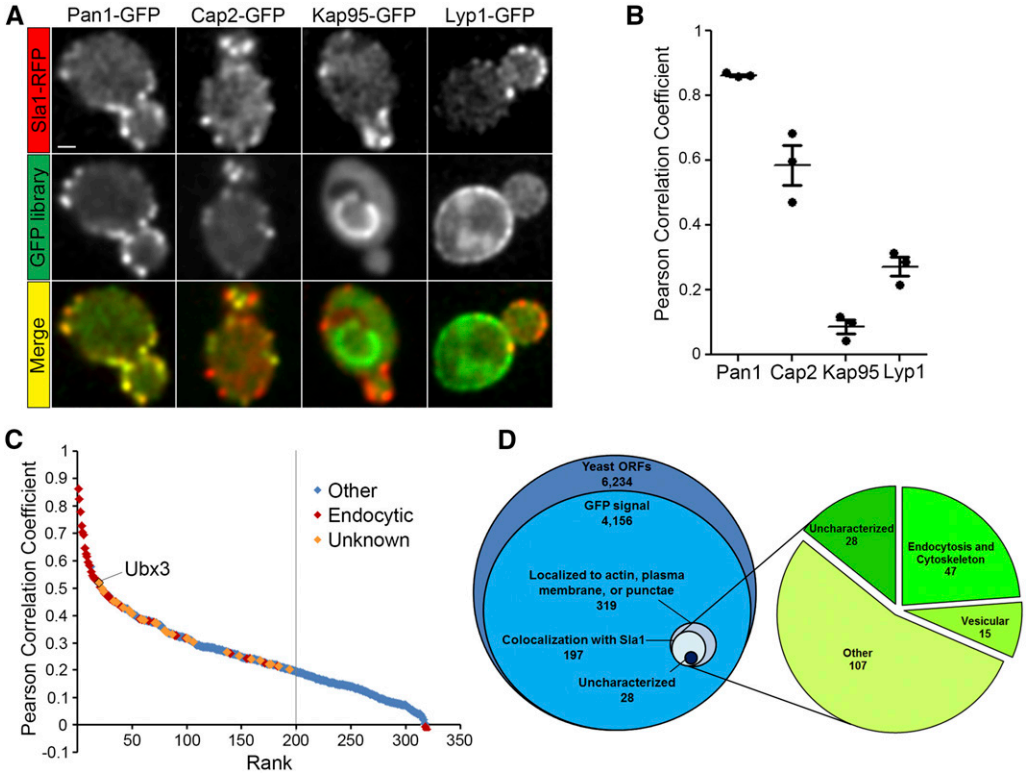

Figure 1 GFP-based screening for endocytic proteins. (A) *S. cerevisiae* cells expressing Sla1–RFP and the indicated GFP-fusion proteins were analyzed by live-cell confocal fluorescence microscopy. Bar, 1 μm. (B) Pearson correlation coefficients (mean ± SD) between Sla1–RFP and each of the proteins demonstrated in A. (C) Distribution of PCC values for Sla1–RFP with the 319 GFP-tagged proteins tested in the screening. Endocytic proteins are indicated with red symbols and uncharacterized proteins with yellow symbols. The cutoff for colocalization (PCC = 0.2) is marked with a line. (D) Left, schematic of how the yeast genome was narrowed down to the 319 proteins selected for the screen. Right, functions of the 197 proteins showing colocalization with Sla1 at a level higher than PCC = 0.2.

modulators of the machinery. Using this strategy we identified a group of uncharacterized endocytic proteins and further study one of them, Ubx3.

Materials and Methods

Plasmids, yeast strains, and GFP library screening

Recombinant GST-fusion Ubx3 protein and fragment containing residues 337–350 (W-box) were created by PCR amplification of full length ORF of genomic DNA or the corresponding fragment and cloning into pGEX-5X-1 (Amersham Biosciences). Recombinant polyhistidine-tagged clathrin heavy chain N-terminal domain was created by PCR amplification of bp 1–1449 of the CHC1 ORF and cloning into pET-30a+ (Novagen). Site-directed mutagenesis was accomplished using the QuikChange system (Stratagene).

The full *Saccharomyces cerevisiae* GFP collection and a strain carrying a deletion of the *UBX3* gene were obtained from Invitrogen (Huh *et al.* 2003). The 319 GFP collection strains selected for the screen were grown in 96-well plates supplied with minimal media. SDY356 (*MAT*α *ura3-52*, *leu2-3,112 his3-Δ200*, *trp1-Δ901*, *lys2-801*, *suc2-Δ9 GAL -MEL chc1-521*::*URA3 SLA1-RFP*::*KAN*) cells were introduced into each well using a replica plater. Mating was allowed for 2 hr at 30°. The replica plater was then used to stamp mated cells from the 96-well plate onto selective media agar plates. Mated cells were allowed to grow for 3 days, returned to liquid media with 15% glycerol, and stored at −80° until imaging as described below. StrainYYH75 (*MAT***a** *ura3-52*, *leu2-3*, *cdc48-3*) carrying the temperature-sensitive allele of the *CDC48* gene and parental strain were a gift from Dr. Tingting Yao. All other strains carrying gene deletions or fluorescent tags were generated following standard approaches and are described in the Supporting Information.

Biochemical methods

Total yeast cell extracts were prepared as described previously (Di Pietro *et al.* 2010; Feliciano *et al.* 2011). GST- and polyhistidine-fusion proteins were expressed in *Escherichea coli* and purified as described (Feliciano *et al.* 2011, 2015). GST-pulldowns were performed by loading glutathione-Sepharose beads with GST-fusion protein (5 μg) for 30 min at room temperature. Beads were washed 2 times to remove excess GST-fusion protein, and then cell extract (1.5 mg) or purified protein (5 μg) in 1 ml of PBS (or 50 mM HEPES, 100 mM NaCl, pH 7.4) containing 1% TritonX-100 was added to beads and rotated for 1 hr at 4°. Beads were washed three times with the same buffer and once with buffer without TritonX-100; 1% of initial protein or extract was loaded to gel for input comparison. One-third of pulldown product was loaded for each sample. Western blotting was performed with Anti-6His (Sigma) or anti-GFP (Payne lab).

Fluorescence microscopy and endocytosis assays

Fluorescence microscopy was performed as described using an Olympus IX81 spinning-disk confocal microscope (Feliciano and Di Pietro 2012). Cells were grown to early log phase and imaged at room temperature except in case of heat shock (37°). Time-lapse images were collected every 2 sec (Figure

Table 1 Uncharacterized proteins colocalizing with Sla1–RFP

Screening rank	Systematic name	Common name	PCC ± SD
20	YDL091C	Ubx3	0.52 ± 0.26
23	YDL012C[a]		0.50 ± 0.14
24	YER071C	TDA2	0.49 ± 0.13
33	YOR104W[b,c]	PIN2	0.45 ± 0.19
36	YGR026W[b]		0.45 ± 0.03
42	YBL029C-A		0.43 ± 0.12
47	YBR016W[a]		0.42 ± 0.05
49	YDR090C[b]		0.41 ± 0.11
50	YDR034W-B[a]		0.41 ± 0.09
58	YDR033W[b]	MRH1	0.39 ± 0.15
61	YMR295C		0.38 ± 0.05
71	YDR344C		0.37 ± 0.05
73	YDR210W[a]		0.37 ± 0.05
80	YLR413W[b]		0.35 ± 0.01
81	YBR052C	RFS1	0.34 ± 0.08
87	YLR407W		0.33 ± 0.10
100	YOL019W[b]	TOS7	0.32 ± 0.08
101	YOR161C[b]	PNS1	0.32 ± 0.11
106	YPL032C	SVL3	0.30 ± 0.05
137	YGL108C[c]		0.27 ± 0.19
148	YDR032C	PST2	0.25 ± 0.08
159	YLR353W[b]	BUD8	0.24 ± 0.11
167	YOL084W[b]	PHM7	0.24 ± 0.22
175	YOL070C	NBA1	0.22 ± 0.11
177	YCR004C[c]	YCP4	0.22 ± 0.17
184	YNL190W[a]		0.22 ± 0.06
194	YBR255W[b]	MTC4	0.20 ± 0.12

[a] Predicted tail-anchor to plasma membrane.
[b] Predicted transmembrane region(s)
[c] Predicted to be palmitoylated.

2) or 5 sec (Figure 4). Slidebook 6 software (3I, Denver, CO) was used for analysis. Lucifer yellow uptake experiments were performed as described (Duncan *et al.* 2001), incubating cells in dye for 2 hr at room temperature (excepting heat shock strains at 37°). Fluorescence was measured with a mask drawn on the vacuole and normalized to the background. Mup1-GFP cells were grown in minimal media with methionine to early log phase, moved to minimal media lacking methionine for 2 hr, and imaged at each time point after return to methionine-rich media. Fluorescence in the membrane was measured using a mask drawn on the cell periphery and normalized to the background. Statistical significance was determined using an unpaired Student's *t*-test (Graphpad Software) comparing mean, SEM, and *N* (cells or patches).

Data Availability

All yeast strains are available upon request.

Results

A GFP-based screening of S. cerevisiae for novel endocytic proteins

We took advantage of the *S. cerevisiae* GFP library, containing the coding sequence of GFP immediately preceding the stop codon of each ORF in the yeast genome (Huh *et al.* 2003). Library proteins are therefore expressed from their endogenous promoter, with a GFP tag at the carboxy-terminal end. Creators of the library performed an initial classification of the subcellular localization for 4156 GFP-tagged proteins representing ~75% of the proteome. We noted that well-established components of the endocytic machinery were found in three localization groups: the plasma membrane, actin, and punctate (Huh *et al.* 2003). Together the three groups contain 319 GFP-tagged proteins and include numerous proteins with unknown function. We reasoned that some of these unknown proteins may specifically localize to sites of endocytosis and constitute new components of the endocytic machinery. To test that possibility, *MAT***a** strains expressing the 319 GFP-tagged proteins in these categories were mated with *MAT*α cells expressing Sla1–RFP from the endogenous locus and resulting diploid cells were selected with appropriate markers. Sla1 is a multifunctional clathrin adaptor and actin polymerization regulator present at all sites of CME and easily visible by fluorescence microscopy (Figure 1A) (Ayscough *et al.* 1999; Kaksonen *et al.* 2003; Kaksonen *et al.* 2005; Di Pietro *et al.* 2010; Feliciano and Di Pietro 2012; Feliciano *et al.* 2015). Each diploid strain expressing both the corresponding GFP-fusion protein and Sla1–RFP was subjected to live cell confocal fluorescence microscopy and colocalization analysis. To ensure an unbiased study, the operator did not know the identity of the strain subjected to imaging and random images were used to determine colocalization levels.

Visual and quantitative data reveal candidate endocytic proteins

The Pearson correlation coefficient (PCC) was determined for each GFP-tagged protein by averaging at least three images, each containing multiple cells with several endocytic patches. The library proteins were then ranked from highest to lowest PCC with a range of 0.86 to −0.02 (Supporting Information, Table S1). Representative examples are shown in Figure 1A. The highest scoring protein, Pan1 (0.86 ± 0.01, mean ± SD), is known to have the same dynamics as Sla1 and therefore expected to display a high colocalization level (Kaksonen *et al.* 2003, 2005; Boettner *et al.* 2012; Weinberg and Drubin 2012). The capping protein β subunit, Cap2 (0.58 ± 0.11, mean ± SD), is a component of the actin network that assembles after the arrival of Sla1 (Kaksonen *et al.* 2005) and shows intermediate level of colocalization. The lysine permease Lyp1 (0.27 ± 0.05, mean ± SD) localizes to the plasma membrane in a relatively uniform manner and thus represents a low colocalization level. A nuclear pore protein classified as punctate localization, Kap95 (0.09 ± 0.04, mean ± SD) serves as an example of background PCC obtained with a noncolocalizing protein (Figure 1, A and B). Based on these observations, proteins with PCC >0.2 were considered to show colocalization above background, totaling 197 of the 319 strains (Figure 1C).

The functions of the 197 colocalizing proteins were obtained from the *Saccharomyces* Genome Database and

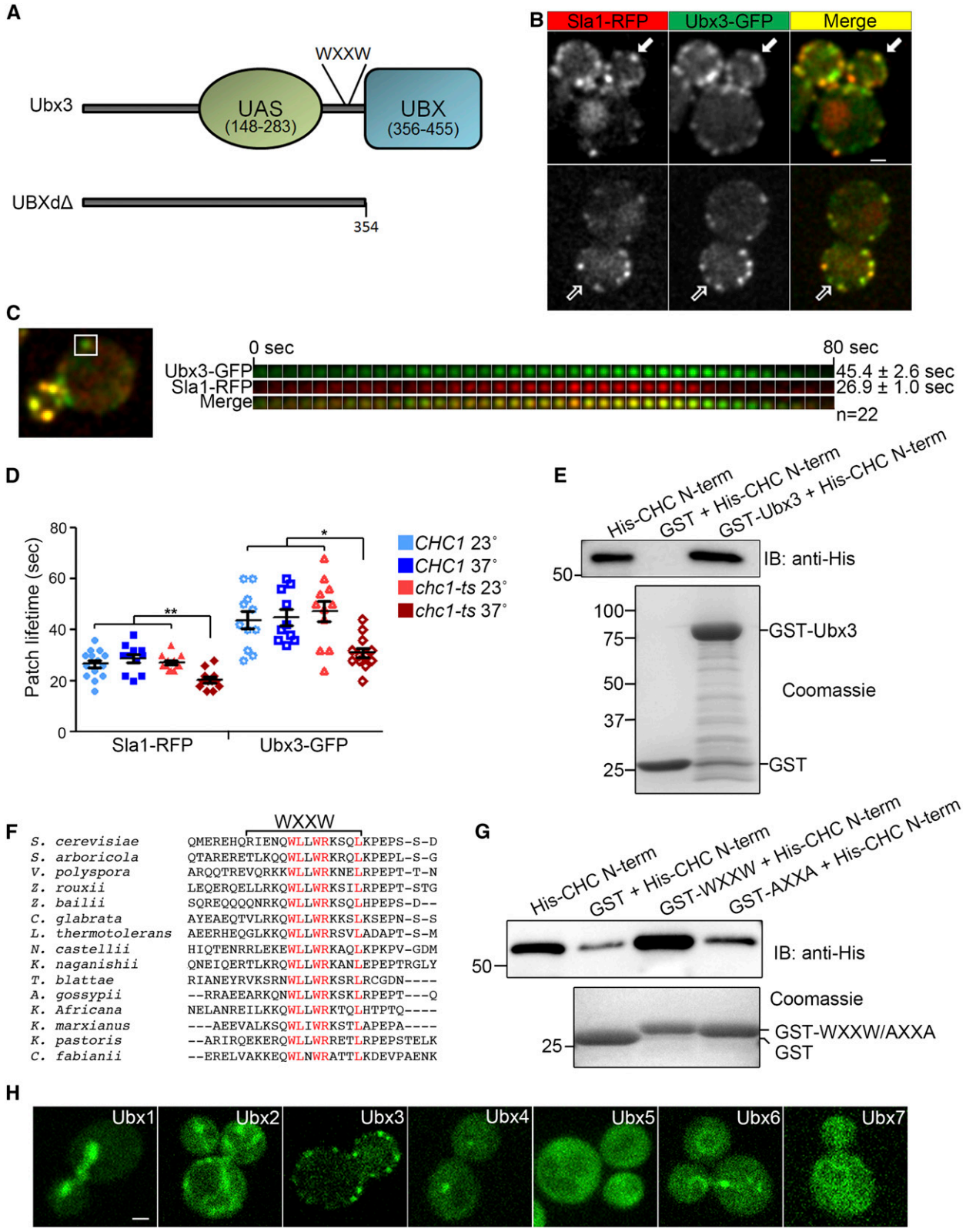

Figure 2 Ubx3 is a novel component of the endocytic machinery. (A) Cartoon representation of Ubx3 domains predicted by the Phyre2 protein-folding recognition engine. UAS, domain of unknown function. (B) Ubx3–GFP shows strong colocalization with Sla1–RFP by live-cell confocal fluorescence microscopy. Solid arrows show an example of an endocytic patch demonstrating strong colocalization; open arrows show an example of Ubx3–GFP present at an endocytic patch without Sla1–RFP. Bar, 1 μm. (C) Dynamics of Ubx3–GFP and Sla1–RFP at endocytic sites were compared. Left, one frame of a movie indicating with a white box the endocytic site used for constructing a kymograph. Right, kymograph demonstrating dynamics of Ubx3–GFP and Sla1–RFP, and average patch lifetimes (22 patches from seven cells, mean ± SEM). Each frame represents 2 sec. (D) Patch lifetimes of Sla1–RFP and

the literature, showing representation from endocytic, cytoskeletal, trafficking, as well as other functions (Figure 1D, Table S1). Of the 45 known endocytic proteins included in the screening, only two (Sac6 and Arp2) fell below the 0.2 PCC cutoff for colocalization, indicating that the group of 197 proteins includes the vast majority of machinery components analyzed in the group of 319 strains (Table S1 and Table S2). Furthermore, 31 of the top 50 PCCs corresponded to well-studied endocytic proteins, such as Sla2, Ent2, and Bbc1. Thus, a majority of the known endocytic machinery proteins were located high in this ranking (Table S1 and Table S2). Interestingly, all four subunits of the AP-2 complex scored a colocalizing PCC, consistent with recent findings that AP-2 does in fact play a role in yeast CME (Carroll *et al.* 2009; Chapa-Y-Lazo *et al.* 2014). The lower range of the 197 colocalizing proteins was enriched in proteins spanning a variety of functions and containing predicted or known transmembrane domains. Such proteins correspond to known or likely CME cargo and typically showed a relatively even distribution throughout the plasma membrane similar to Lyp1 (Figure 1A and Table S1). To identify probable new machinery components, we next focused on proteins with unknown function and PCC similar to known endocytic proteins.

Importantly, 28 uncharacterized proteins colocalize with Sla1 and many of them are not predicted to have a transmembrane domain and thus may not be endocytic cargo (Figure 1, C and D and Table 1). Most notably, nine of such uncharacterized proteins were in the top 50 PCC scores, representing highly likely new components of the endocytic machinery. The highest scoring uncharacterized protein was Ubx3 with a PCC of 0.52 ± 0.20 (Figure 1C, Table S1, and Table 1). This protein was identified as having a punctate composite fluorescent pattern in the library, which also showed a higher cytosolic background compared to our images, probably due to their use of wide-field fluorescence microscopy. Ubx3 is defined by a ubiquitin-like UBX (ubiquitin regulatory X) domain in its C terminus (Figure 2A) (Dreveny *et al.* 2004; Schuberth *et al.* 2004; Schuberth and Buchberger 2008) and was subjected to further study to confirm its endocytic role.

Ubx3 is the first UBX domain-containing protein in the endocytic machinery

By confocal fluorescence microscopy, Ubx3–GFP displayed similar patch dynamics to Sla1–RFP and other endocytic coat proteins arriving at intermediate stages. Ubx3–GFP had a patch lifetime of 45 ± 3 sec, appearing slightly before Sla1–RFP at the endocytic site and remaining slightly after the disappearance of Sla1–RFP (Figure 2, B and C and File S1). Ubx3–GFP is recruited after early coat proteins such as Ede1–RFP (Figure S1). Ubx3–GFP patches also showed movement away from the surface toward the center of the cell right before disappearing, a behavior typical of endocytic coat proteins (Figure 2C, last eight frames, and File S1). To assess whether Ubx3–GFP patch localization is affected by the endocytic coat, Ubx3–GFP dynamics was visualized in cells carrying a temperature-sensitive allele of the clathrin heavy-chain gene (*chc1-ts*) (Bensen *et al.* 2000). Upon incubation at 37°, the patch lifetime of Ubx3–GFP was significantly reduced (Figure 2D). In contrast, the patch lifetime of Ubx3–GFP in wild-type cells (*CHC1*) was not affected by incubation at 37° (Figure 2D). For comparison, the clathrin-binding adaptor protein Sla1–GFP (Di Pietro *et al.* 2010) was analyzed in parallel in cells carrying the *chc1-ts* allele and demonstrated a similar reduction in patch lifetime upon incubation at 37°, whereas wild-type cells did not (Figure 2D). This result indicates that Ubx3 associates with the endocytic coat *in vivo*. To investigate whether Ubx3 binds clathrin, we tested *in vitro* for physical interaction by GST pulldown. GST and GST–Ubx3 were immobilized on glutathione-Sepharose beads and incubated with polyhistidine-tagged clathrin heavy-chain N-terminal β-propeller domain (His–CHC N-term) (Kirchhausen *et al.* 2014). Immunoblotting analysis showed binding of His–CHC N-term to GST–Ubx3 but not to GST indicating a direct physical interaction (Figure 2E). Inspection of the Ubx3 amino acid sequence for clathrin-binding motifs revealed no obvious clathrin-box (LLDLD related sequence) (Dell'Angelica *et al.* 1998). However, a sequence conforming to the core W-box motif (W*X*X*X*W), where *X* represents any amino acid (Ramjaun and Mcpherson 1998; Miele *et al.* 2004), was located upstream the UBX domain (Figure 2A). Sequence alignment revealed that these residues are extremely well conserved among the Ubx3 family, suggesting functional importance (Figure 2F). Consistent with a functional W-box capable of engaging the clathrin β-propeller domain, this stretch of the Ubx3 sequence is predicted to be disordered. The ability of this sequence to bind clathrin was determined by GST-pulldown. A GST-fusion protein containing the Ubx3 candidate W-box and flanking sequences (residues 337–350, GST–W*X*X*X*W) bound His–CHC N-term significantly above background levels (GST) (Figure 2G).

Ubx3–GFP were measured at room temperature and 37° in both wild-type (*CHC1*) and temperature-sensitive clathrin heavy-chain (*chc1-ts*) cells (15 patches from 5 cells per strain and temperature, mean ± SEM; **, $P < 0.0001$; *, $P < 0.001$). (E) GST–Ubx3 directly binds polyhistidine-tagged clathrin heavy-chain N-terminal domain as determined by GST-pulldown with purified proteins. Top: eluted proteins were analyzed by immunoblotting using an antibody to the polyhistidine tag (anti-His). Bottom: loading control Coomassie-stained gel of GST and GST–Ubx3 proteins bound to glutathione beads. (F) Alignment of *S. cerevisiae* Ubx3 amino acid sequence with that of other fungal species demonstrates high conservation of residues matching the W-box core clathrin-binding motif. Strictly conserved residues are shown in red. The fragment fused to GST for GST-pulldown assays in Figure 2G is indicated at the top (W*X*X*X*W). (G) Ubx3 contains a W-box that binds the clathrin heavy-chain N-terminal domain. GST alone, GST–W*X*X*X*W, and corresponding mutant GST–A*X*X*X*A were bound to glutathione-Sepharose beads and incubated with polyhistidine-tagged N-terminal domain of clathrin heavy chain. The eluted proteins were analyzed by immunoblotting using an antibody to the polyhistidine tag (anti-His). Bottom: loading control Coomassie-stained gel of GST-fusion proteins bound to glutathione beads. (H) Ubx3–GFP is the only UBX domain-containing protein that localizes to endocytic patches. Yeast strains expressing each of the seven Ubx proteins tagged with GFP were analyzed by confocal fluorescence microscopy. Bar, 1 μm.

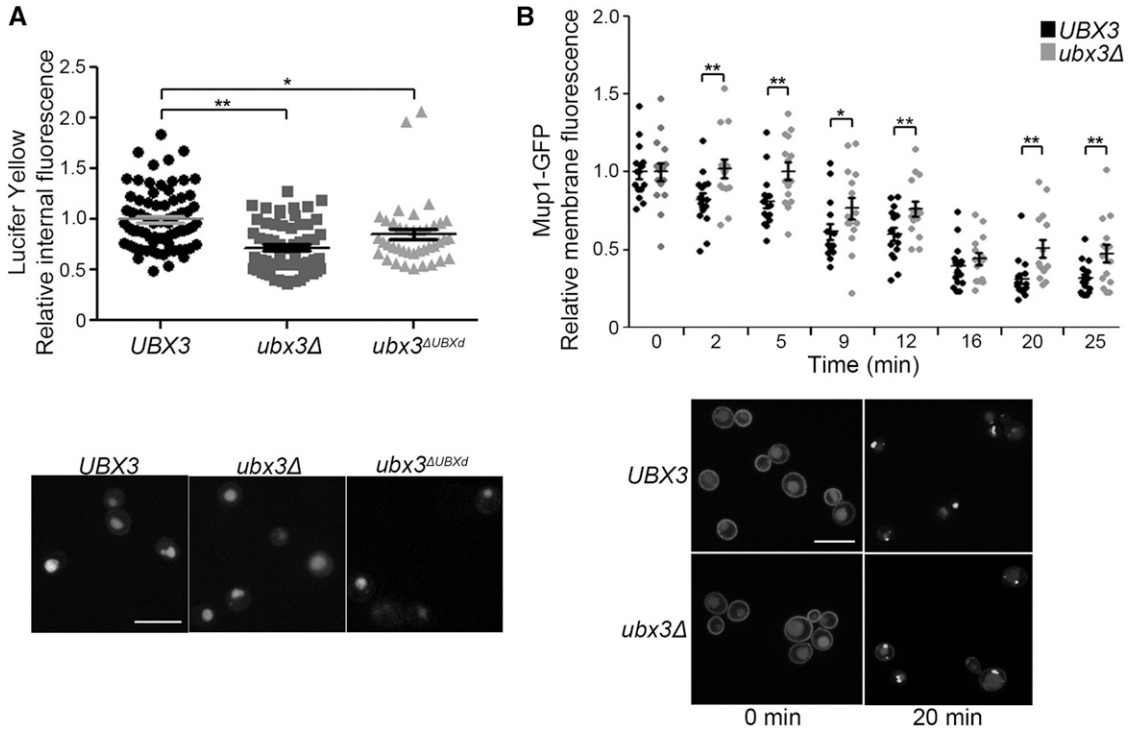

Figure 3 Ubx3 is needed for optimal endocytosis. (A) Wild-type cells (*UBX3*) and cells carrying a deletion of the *UBX3* gene (*ubx3Δ*) and a deletion of the UBX domain in the *UBX3* gene (*ubx3*$^{\Delta UBXd}$) were incubated with Lucifer yellow and imaged by confocal fluorescence microscopy. The fluorescence intensity inside the cell was measured, normalized by the intensity of the background, and expressed as the average relative fluorescence intensity (40 cells per strain, mean ± SEM; **, $P < 0.001$; *, $P < 0.01$). The experiment was performed two times with similar results. Bottom: representative images of the cells. Bar, 10 μm. (B) Endocytosis of the methionine transporter Mup1 tagged with GFP was analyzed in *UBX3* and *ubx3Δ* cells as described in *Materials and Methods*. Fluorescence in the plasma membrane was measured using a mask drawn on the cell periphery and normalized to the background (15 cells per strain and time point, mean ± SEM; **, $P < 0.001$; *, $P < 0.01$). The experiment was performed three times with similar results. Bottom: representative images of cells at 0 and 20 min after change to media containing methionine. Bar, 10 μm.

Mutation of the tryptophan residues to alanine (GST–A*XX*A) diminished His–CHC N-term binding to background levels, showing that binding was specific (Figure 2G). To our knowledge, this is the first example of a W-box type clathrin-binding motif in a nonmammalian protein. Together these results demonstrate Ubx3 binds clathrin and that it is a component of the endocytic coat. As there are seven UBX domain-containing proteins in yeast, we visualized each protein tagged with GFP to determine if any others localized to endocytic sites, but only Ubx3 displayed an endocytic punctate fluorescent pattern (Figure 2H).

To further test for a role of Ubx3 in endocytosis we performed two uptake assays. First we used Lucifer yellow, a fluid-phase fluorescent dye, to track bulk intake into cells. Wild-type cells and cells carrying a deletion of the *UBX3* gene (*ubx3Δ*) were incubated with media containing Lucifer yellow and the internalized dye was quantified by fluorescence microscopy. An internalization defect was observed for *ubx3Δ* cells compared to wild-type cells (Figure 3A). The extent of the defect was comparable to the one we observed for Las17-MP8-12, a mutant displaying altered Las17 recruitment to endocytic sites and misregulation of actin polymerization (Feliciano and Di Pietro 2012). We also developed a strain harboring a deletion of the UBX domain in the endogenous *UBX3* gene (*ubx3*$^{\Delta UBXd}$) (Figure 2A). This strain displayed a similar defect in Lucifer yellow internalization, suggesting that Ubx3 depends on its UBX domain for endocytic function (Figure 3A). GFP tagging of the *ubx3*$^{\Delta UBXd}$ allele and live cell imaging showed that the mutant Ubx3 protein is not degraded but localizes to fast-moving internal structures rather than endocytic sites (File S2). Thus, the UBX domain is required for normal Ubx3 localization and function at endocytic sites. We then used Mup1–GFP to track cargo endocytosis. Mup1 is a methionine transporter that is expressed at the plasma membrane when cells are starved for methionine, but quickly internalized via ubiquitin-dependent CME when cells are returned to methionine-rich media. Internalization of this cargo again portrayed a delay in *ubx3Δ* cells compared to wild-type cells (Figure 3B). Together, these data demonstrate that Ubx3 is a new component of the clathrin-mediated endocytic machinery needed for optimal endocytosis (see File S3).

Ubx3 regulates dynamics of the early arriving protein Ede1 but not later arriving coat proteins or actin assembly

In an effort to understand the mechanistic basis of Ubx3 function in CME, we examined the patch lifetimes of known endocytic proteins tagged with GFP in wild-type and *ubx3Δ*

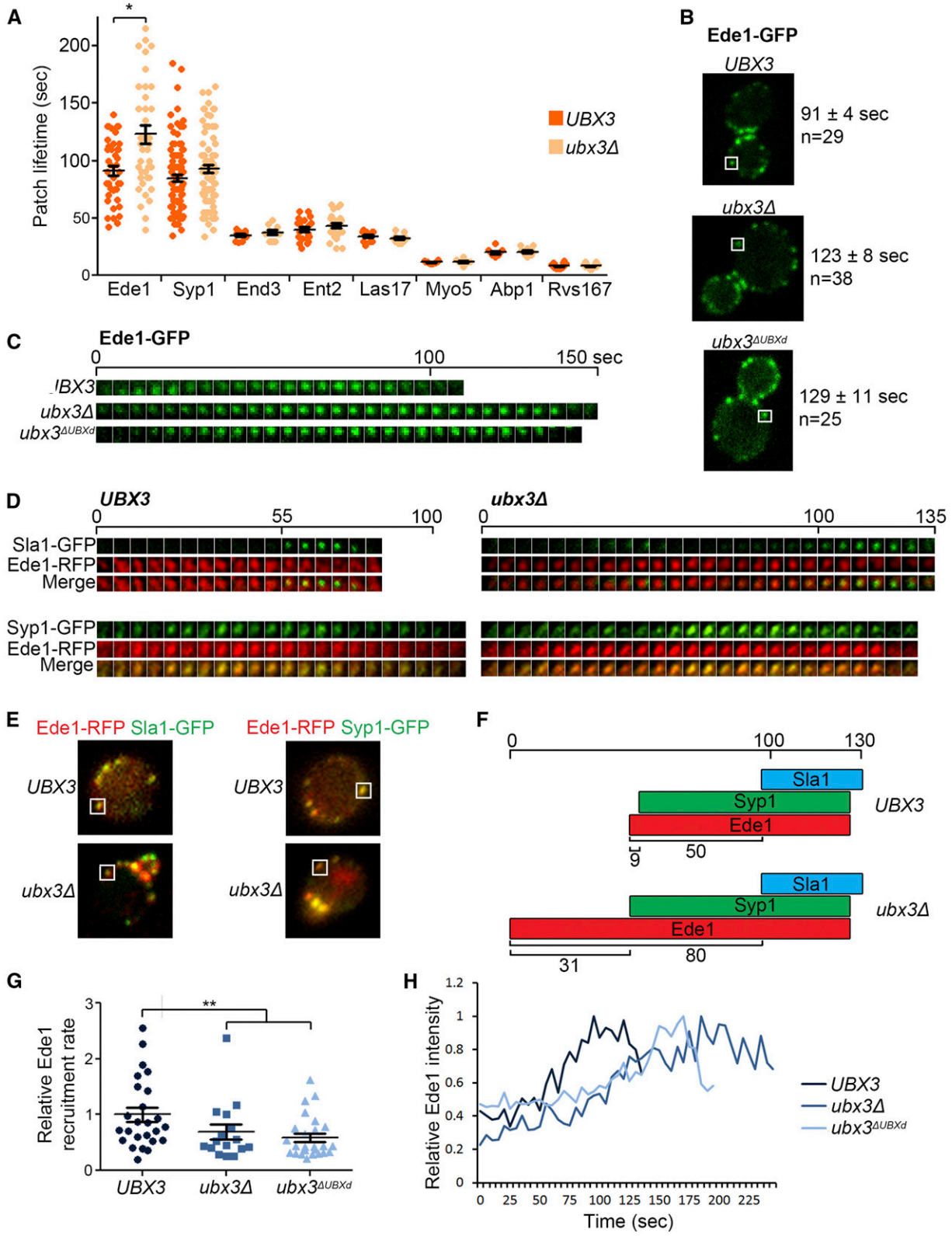

Figure 4 Ede1 dynamics at sites of endocytosis depend on Ubx3. (A) Ede1–GFP has a large increase in endocytic patch lifetime in *ubx3Δ* cells, while other endocytic machinery proteins tested are unaffected. Strains expressing the indicated GFP-tagged proteins either in *UBX3* or *ubx3Δ* background were analyzed by live-cell fluorescence microscopy (10–58 patches from four or more cells per strain, mean ± SEM; *, $P < 0.01$). (B) Frames from movies of cells expressing Ede1–GFP in *UBX3*, *ubx3Δ*, or $ubx3^{\Delta UBXd}$ background. Boxed patches are tracked in the kymographs shown in C. Ede1–GFP patch lifetime (mean ± SEM) and number of patches analyzed for each strain are shown on the right (at least 10 cells per strain were analyzed). (C) Kymographs demonstrating the increase in Ede1–GFP lifetime in *ubx3Δ* cells and $ubx3^{\Delta UBXd}$ cells compared to *UBX3* cells. Each frame represents

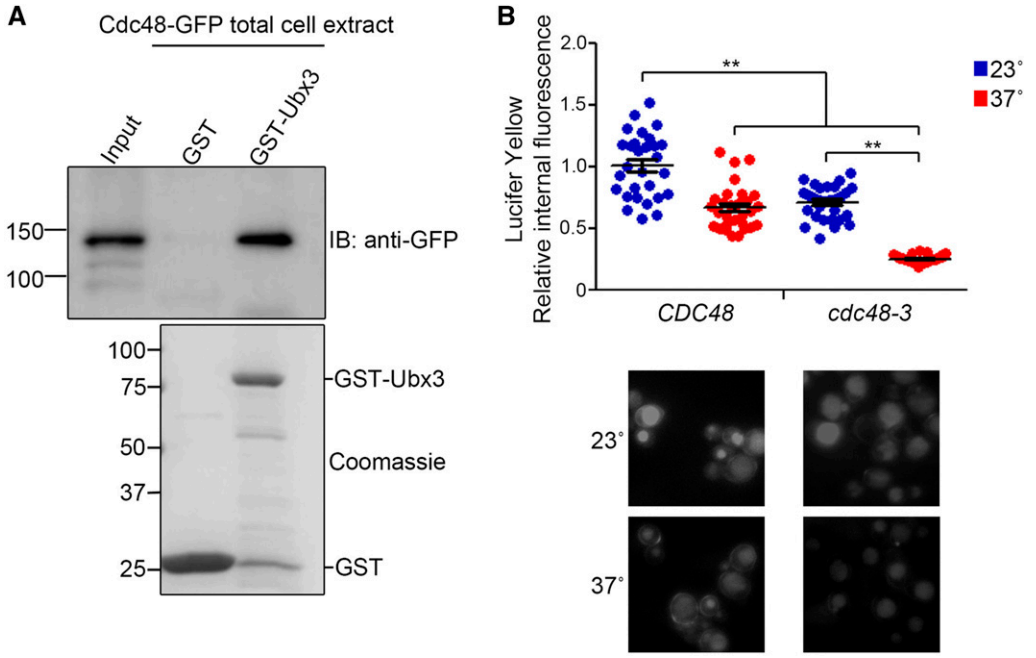

Figure 5 Ubx3 interacts physically with Cdc48 and endocytosis depends on Cdc48. (A) Ubx3 binds Cdc48. GST–Ubx3 and GST alone were bound to glutathione-Sepharose beads and incubated with total cell extract prepared with a strain expressing Cdc48–GFP from the endogenous locus. The eluted proteins were analyzed by immunoblotting using an antibody to the GFP tag (anti-GFP). Bottom: loading control Coomassie-stained gel of GST and GST–Ubx3 proteins bound to glutathione beads in the assay. (B) Lucifer yellow uptake was measured at room temperature and 37° in both wild-type cells (*CDC48*) and cells carrying a temperature-sensitive allele of the *CDC48* gene (*cdc48-3*). The fluorescence intensity inside the cell was measured, normalized by the intensity of the background, and expressed as the average relative fluorescence intensity (30 cells per strain, mean ± SEM; **, $P < 0.0001$). Bottom: representative images of the cells.

cells. We analyzed early (Ede1, Syp1), intermediate (End3, Ent2, Las17), and late (Myo5, Abp1, Rvs167) arriving components of the endocytic machinery (Kaksonen *et al.* 2005; Toshima *et al.* 2006; Boettner *et al.* 2009, 2012; Reider *et al.* 2009; Stimpson *et al.* 2009; Weinberg and Drubin 2012; Brach *et al.* 2014). Remarkably, Ede1–GFP had a significantly longer patch lifetime in *ubx3Δ* cells compared to wild-type cells while other endocytic proteins were unaffected (Figure 4, A–C). Ede1–GFP displayed a 34% increase in lifetime from 91 ± 4 sec to 123 ± 8 sec (mean ± SEM, $P < 0.01$) (Figure 4, A–C). Analysis of $ubx3^{\Delta UBXd}$ cells demonstrated a similar increase in Ede1–GFP lifetime (129 ± 11 sec, mean ± SEM, $P < 0.01$), again establishing that the UBX domain is required for Ubx3 function (Figure 4, B and C). The extension of the Ede1 patch lifetime occurs at the beginning of the endocytic process, as the time between arrival of Ede1–RFP and Sla1–GFP increases in *ubx3Δ* cells compared to wild-type cells (Figure 4, D–F). A similar delay was observed between the arrival of Ede1–RFP and Syp1–GFP in *ubx3Δ* cells compared to wild-type cells (Figure 4, D–F). The cause of this delay appeared to be a slower recruitment of Ede1–GFP to the endocytic site as we noted that in *ubx3Δ* cells and $ubx3^{\Delta UBXd}$ cells Ede1–GFP fluorescence intensity increased more slowly before reaching the peak (Figure 4C). Indeed, quantification of the Ede1–GFP relative recruitment rate demonstrated a significant defect in *ubx3Δ* cells and $ubx3^{\Delta UBXd}$ cells compared to wild-type cells (Figure 4, G and H). Slower Ede1 recruitment and prolonged endocytic patch lifetime in *ubx3Δ* cells and $ubx3^{\Delta UBXd}$ cells further link Ubx3 to the CME machinery and is consistent with the Lucifer yellow and Mup1–GFP endocytosis defects shown above.

Given the effect of *UBX3* gene deletion on the dynamics and patch lifetime of Ede1–GFP, we examined the converse relationship. The Ubx3–GFP patch lifetime was determined in wild-type and *ede1Δ* cells. Ubx3–GFP displayed a significant decrease in patch lifetime from 43 ± 2 sec to 31 ± 3 sec (mean ± SEM, $P < 0.01$) suggesting a functional connection between Ubx3 and Ede1 (Figure S2).

Interestingly, UBX domain-containing proteins constitute a major family of cofactors for the ubiquitin-editing complex Cdc48 that determine its location and targets (Schuberth *et al.* 2004; Schuberth and Buchberger 2008; Stolz *et al.* 2011; Meyer *et al.* 2012; Buchberger 2013). A previous study reported that all seven *S. cerevisiae* UBX domain-containing proteins bind Cdc48 by yeast-two-hybrid analysis (Schuberth *et al.* 2004). We confirmed a physical interaction between Ubx3 and Cdc48 using a GST-pulldown assay (Figure 5A). To test for a function of Cdc48 in endocytosis we used the Lucifer yellow uptake assay with wild-type cells (*CDC48*) and cells carrying a temperature-sensitive allele (*cdc48-3*)

5 sec. D Kymographs displaying the patch lifetime of Ede1–RFP is extended at the beginning of the endocytic process, before Syp1–GFP or Sla1–GFP arrive. Each frame represents 5 sec. (E) Frames from the movies used to construct the kymographs shown in D, with the corresponding endocytic patches indicated by white boxes. (F) Cartoon representation of the Sla1, Syp1, and Ede1 relative timing of arrival to endocytic sites in *UBX3* and *ubx3Δ* cells. (G and H) The recruitment rate of Ede1–GFP, measured from first appearance to peak patch intensity, is slower in *ubx3Δ* and $ubx3^{\Delta UBXd}$ cells compared to *UBX3* cells (25 patches from 8 or more cells per strain, mean ± SEM; **, $P < 0.0001$). The peak fluorescence intensity between strains was unchanged.

(Ye *et al.* 2001). A defect in Lucifer yellow uptake was observed at 37°, indicating a function for Cdc48 in endocytosis (Figure 5B). Therefore Ubx3 function in endocytosis may be linked to the ubiquitin-editing complex Cdc48.

Discussion

We utilized a new microscopy-based screening method to detect highly likely novel components of the CME machinery in *S. cerevisiae*. The proteins found here were not identified in previous screenings for endocytic proteins (Huh *et al.* 2003; Burston *et al.* 2009). Results from the screen should provide a valuable resource for the endocytosis and membrane transport community. Among proteins with unknown function, the top-scoring one, Ubx3, was confirmed as a new regulator of endocytosis using several approaches. The relatively modest nature of the endocytic defects observed in *ubx3Δ* cells may explain why this protein has not been identified in previous screenings. It is also possible that while not normally localized to CME sites, other UBX proteins do play a compensatory role in *ubx3Δ* cells. Additional proteins with unknown function, particularly those displaying high PCC in the screen, are likely *bona fide* regulators of endocytosis. Indeed we have confirmed that the third highest scoring protein, YER071C, is a new CME machinery component and will report its characterization in detail elsewhere. Characterization of the other top-scoring proteins identified here will likely shed new light on the CME regulatory mechanisms in *S. cerevisiae*. Given the high conservation of the CME machinery during evolution, the new proteins identified here likely regulate endocytosis not only in yeast but also in other eukaryotes.

Our data revealed Ubx3 as the first member of the conserved UBX domain protein family with a function in endocytosis. Ubx3 is a component of the coat that interacts physically and functionally with clathrin and regulates endocytosis. Of note, Ubx3 represents the first example of a non-mammalian protein containing a W-box indicating that this clathrin-binding mode is ancient. Because deletion of the *UBX3* gene affected both bulk endocytosis (Lucifer yellow) and internalization of a specific cargo (Mup1–GFP), we favor a model in which Ubx3 functions as a general CME factor rather than a cargo-specific adaptor.

At a mechanistic level, Ubx3 regulates the patch dynamics of Ede1, one of the earliest arriving components and known to regulate endocytic site initiation (Toshima *et al.* 2006; Dores *et al.* 2010; Brach *et al.* 2014). Different scenarios could explain this result. First, it is possible that Ubx3 is present early on with Ede1 at endocytic sites at levels low enough that it is not detected until later when more molecules accumulate. We consider this possibility unlikely, but cannot rule it out. Second, Ede1 may begin to assemble normally, but only later stages of recruitment depend on Ubx3. Third, Ubx3 may act indirectly on Ede1 dynamics. Ede1 is subjected to ubiquitination and deubiquitination and alteration of this dynamic was previously shown to affect Ede1 recruitment to the membrane (Dores *et al.* 2010; Weinberg and Drubin 2014). Thus, we speculate that Ubx3 may regulate the balance of Ede1 ubiquitination/deubiquitination and consequently Ede1 dynamics at CME sites. Fourth, Ubx3 may function in endocytosis by regulating the ubiquitination of integral membrane protein cargo at endocytic sites or even downstream at endosomes. In such a scenario the extension of Ede1 patch lifetime in *ubx3Δ* cells would be secondary to cargo misregulation. In either of the last two scenarios, ubiquitin modifications of Ede1 or cargo are involved. The fact that Ubx3 binds to the ubiquitin-editing complex Cdc48 and that inactivation of Cdc48 affects endocytosis supports a function of Ubx3 in ubiquitin regulation at endocytic sites. Elucidating exactly how Ubx3 regulates endocytosis warrants future experimentation.

In summary, through our screening we have provided evidence for novel, uncharacterized proteins as components of the CME machinery. Furthermore, these studies establish a new paradigm for UBX domain protein function as a regulator of endocytic site progression.

Acknowledgments

We thank Al Aradi for help with protein purification, Colette Worcester for help with PCR, Tingting Yao for *cdc48-3* strain, Laurie Stargell for *ubx3Δ* cells, and Greg Payne for anti-GFP antibody. This work was supported by National Science Foundation grant 1052188. K.B.F. acknowledges American Heart Association predoctoral fellowship. Microscopes used in this work are supported in part by the Microscope Imaging Network core infrastructure grant from Colorado State University. The authors declare that they have no conflict of interest.

Literature Cited

Ayscough, K. R., J. J. Eby, T. Lila, H. Dewar, K. G. Kozminski *et al.*, 1999 Sla1p is a functionally modular component of the yeast cortical actin cytoskeleton required for correct localization of both Rho1p-GTPase and Sla2p, a protein with talin homology. Mol. Biol. Cell 10: 1061–1075.

Bensen, E. S., G. Costaguta, and G. S. Payne, 2000 Synthetic genetic interactions with temperature-sensitive clathrin in *Saccharomyces cerevisiae*: roles for synaptojanin-like Inp53p and dynamin-related Vps1p in clathrin-dependent protein sorting at the trans-Golgi network. Genetics 154: 83–97.

Boettner, D. R., J. L. D'Agostino, O. T. Torres, K. Daugherty-Clarke, A. Uygur *et al.*, 2009 The F-BAR protein Syp1 negatively regulates WASp-Arp2/3 complex activity during endocytic patch formation. Curr. Biol. 19: 1979–1987.

Boettner, D. R., R. J. Chi, and S. K. Lemmon, 2012 Lessons from yeast for clathrin-mediated endocytosis. Nat. Cell Biol. 14: 2–10.

Brach, T., C. Godlee, I. Moeller-Hansen, D. Boeke, and M. Kaksonen, 2014 The initiation of clathrin-mediated endocytosis is mechanistically highly flexible. Curr. Biol. 24: 548–554.

Buchberger, A., 2013 Roles of Cdc48 in regulated protein degradation in yeast. Subcell. Biochem. 66: 195–222.

Burston, H. E., L. Maldonado-Baez, M. Davey, B. Montpetit, C. Schluter *et al.*, 2009 Regulators of yeast endocytosis identified by systematic quantitative analysis. J. Cell Biol. 185: 1097–1110.

Carroll, S. Y., P. C. Stirling, H. E. Stimpson, E. Giesselmann, M. J. Schmitt *et al.*, 2009 A yeast killer toxin screen provides insights into a/b toxin entry, trafficking, and killing mechanisms. Dev. Cell 17: 552–560.

Chapa-y-Lazo, B., E. G. Allwood, I. I. Smaczynska-de Rooij, M. L. Snape, and K. R. Ayscough, 2014 Yeast endocytic adaptor AP-2 binds the stress sensor Mid2 and functions in polarized cell responses. Traffic 15: 546–557.

Dell'Angelica, E. C., J. Klumperman, W. Stoorvogel, and J. S. Bonifacino, 1998 Association of the AP-3 adaptor complex with clathrin. Science 280: 431–434.

Di Pietro, S. M., D. Cascio, D. Feliciano, J. U. Bowie, and G. S. Payne, 2010 Regulation of clathrin adaptor function in endocytosis: novel role for the SAM domain. EMBO J. 29: 1033–1044.

Dores, M. R., J. D. Schnell, L. Maldonado-Baez, B. Wendland, and L. Hicke, 2010 The function of yeast epsin and Ede1 ubiquitin-binding domains during receptor internalization. Traffic 11: 151–160.

Dreveny, I., H. Kondo, K. Uchiyama, A. Shaw, X. Zhang *et al.*, 2004 Structural basis of the interaction between the AAA ATPase p97/VCP and its adaptor protein p47. EMBO J. 23: 1030–1039.

Duncan, M. C., M. J. Cope, B. L. Goode, B. Wendland, and D. G. Drubin, 2001 Yeast Eps15-like endocytic protein, Pan1p, activates the Arp2/3 complex. Nat. Cell Biol. 3: 687–690.

Feliciano, D., and S. M. Di Pietro, 2012 SLAC, a complex between Sla1 and Las17, regulates actin polymerization during clathrin-mediated endocytosis. Mol. Biol. Cell 23: 4256–4272.

Feliciano, D., J. J. Bultema, A. L. Ambrosio, and S. M. Di Pietro, 2011 In vivo and in vitro studies of adaptor-clathrin interaction. J. Vis. Exp. 47: pii: 2352. DOI: 10.3791/2352.

Feliciano, D., T. O. Tolsma, K. B. Farrell, A. Aradi, and S. M. Di Pietro, 2015 A second Las17 monomeric actin-binding motif functions in Arp2/3-dependent actin polymerization during endocytosis. Traffic 16: 379–397.

Huh, W. K., J. V. Falvo, L. C. Gerke, A. S. Carroll, R. W. Howson *et al.*, 2003 Global analysis of protein localization in budding yeast. Nature 425: 686–691.

Idrissi, F. Z., A. Blasco, A. Espinal, and M. I. Geli, 2012 Ultrastructural dynamics of proteins involved in endocytic budding. Proc. Natl. Acad. Sci. USA 109: E2587–E2594.

Kaksonen, M., Y. Sun, and D. G. Drubin, 2003 A pathway for association of receptors, adaptors, and actin during endocytic internalization. Cell 115: 475–487.

Kaksonen, M., C. P. Toret, and D. G. Drubin, 2005 A modular design for the clathrin- and actin-mediated endocytosis machinery. Cell 123: 305–320.

Kirchhausen, T., D. Owen, and S. C. Harrison, 2014 Molecular structure, function, and dynamics of clathrin-mediated membrane traffic. Cold Spring Harb. Perspect. Biol. 6: a016725.

Kukulski, W., M. Schorb, M. Kaksonen, and J. A. Briggs, 2012 Plasma membrane reshaping during endocytosis is revealed by time-resolved electron tomography. Cell 150: 508–520.

McMahon, H. T., and E. Boucrot, 2011 Molecular mechanism and physiological functions of clathrin-mediated endocytosis. Nat. Rev. Mol. Cell Biol. 12: 517–533.

Merrifield, C. J., and M. Kaksonen, 2014 Endocytic accessory factors and regulation of clathrin-mediated endocytosis. Cold Spring Harb. Perspect. Biol. 6: a016733.

Meyer, H., M. Bug, and S. Bremer, 2012 Emerging functions of the VCP/p97 AAA-ATPase in the ubiquitin system. Nat. Cell Biol. 14: 117–123.

Miele, A. E., P. J. Watson, P. R. Evans, L. M. Traub, and D. J. Owen, 2004 Two distinct interaction motifs in amphiphysin bind two independent sites on the clathrin terminal domain beta-propeller. Nat. Struct. Mol. Biol. 11: 242–248.

Ramjaun, A. R., and P. S. McPherson, 1998 Multiple amphiphysin II splice variants display differential clathrin binding: identification of two distinct clathrin-binding sites. J. Neurochem. 70: 2369–2376.

Reider, A., and B. Wendland, 2011 Endocytic adaptors–social networking at the plasma membrane. J. Cell Sci. 124: 1613–1622.

Reider, A., S. L. Barker, S. K. Mishra, Y. J. Im, L. Maldonado-Baez *et al.*, 2009 Syp1 is a conserved endocytic adaptor that contains domains involved in cargo selection and membrane tubulation. EMBO J. 28: 3103–3116.

Robertson, A. S., E. Smythe, and K. R. Ayscough, 2009 Functions of actin in endocytosis. Cell. Mol. Life Sci. 66: 2049–2065.

Schuberth, C., and A. Buchberger, 2008 UBX domain proteins: major regulators of the AAA ATPase Cdc48/p97. Cell. Mol. Life Sci. 65: 2360–2371.

Schuberth, C., H. Richly, S. Rumpf, and A. Buchberger, 2004 Shp1 and Ubx2 are adaptors of Cdc48 involved in ubiquitin-dependent protein degradation. EMBO Rep. 5: 818–824.

Stimpson, H. E., C. P. Toret, A. T. Cheng, B. S. Pauly, and D. G. Drubin, 2009 Early-arriving Syp1p and Ede1p function in endocytic site placement and formation in budding yeast. Mol. Biol. Cell 20: 4640–4651.

Stolz, A., W. Hilt, A. Buchberger, and D. H. Wolf, 2011 Cdc48: a power machine in protein degradation. Trends Biochem. Sci. 36: 515–523.

Toshima, J. Y., J. Toshima, M. Kaksonen, A. C. Martin, D. S. King *et al.*, 2006 Spatial dynamics of receptor-mediated endocytic trafficking in budding yeast revealed by using fluorescent alpha-factor derivatives. Proc. Natl. Acad. Sci. USA 103: 5793–5798.

Weinberg, J., and D. G. Drubin, 2012 Clathrin-mediated endocytosis in budding yeast. Trends Cell Biol. 22: 1–13.

Weinberg, J. S., and D. G. Drubin, 2014 Regulation of clathrin-mediated endocytosis by dynamic ubiquitination and deubiquitination. Curr. Biol. 24: 951–959.

Ye, Y., H. H. Meyer, and T. A. Rapoport, 2001 The AAA ATPase Cdc48/p97 and its partners transport proteins from the ER into the cytosol. Nature 414: 652–656.

Communicating editor: D. J. Lew

GENETICS

Supporting Information
www.genetics.org/lookup/suppl/doi:10.1534/genetics.115.180729/-/DC1

New Regulators of Clathrin-Mediated Endocytosis Identified in *Saccharomyces cerevisiae* by Systematic Quantitative Fluorescence Microscopy

Kristen B. Farrell, Caitlin Grossman, and Santiago M. Di Pietro

DOI: 10.1534/genetics.115.180729

Supporting Information

New regulators of clathrin-mediated endocytosis identified in *Saccharomyces cerevisiae* by systematic quantitative fluorescence microscopy

Kristen B. Farrell, Caitlin Grossman, and Santiago M. Di Pietro

Files S1-S2

Available for download as .mp4 files at www.genetics.org/lookup/suppl/doi:10.1534/genetics.115.180729/-/DC1

File S3

Supplementary Materials and Methods

Yeast strains

SDY 356 and SDY427 (*MAT*α *ura3-52, leu2-3,112 his3-Δ200, trp1-Δ901, lys2-801, suc2-Δ9 GAL-MEL chc1-521::URA3 UBX3-GFP::HIS3*) were employed for imaging in Figure 2C. SDY500 (*MATα his3Δ1, leu2Δ0, met15-Δ0, ura3 Δ0, trp1-Δ901 ubx3Δ::URA3*) was created, mated with various strains from the GFP library and subsequently sporulated and subjected to tetrad dissection to generate haploid strains SDY586 (*MAT his3Δ1, leu2Δ0, met15-Δ0, ura3 Δ0 ubx3Δ::URA3, MUP1-GFP::HIS3*), SDY567 (*MAT his3Δ1, leu2Δ0, met15-Δ0, ura3 Δ0 ubx3Δ::URA3, EDE1-GFP::HIS3*), SDY569 (*MAT his3Δ1, leu2Δ0, met15-Δ0, ura3 Δ0 ubx3Δ::URA3, ENT2-GFP::HIS3*), SDY570 (*MAT his3Δ1, leu2Δ0, met15-Δ0, ura3 Δ0 ubx3Δ::URA3, RVS167-GFP::HIS3*), and SDY585 (*MAT his3Δ1, leu2Δ0, met15-Δ0, ura3 Δ0 ubx3Δ::URA3, SYP1-GFP::HIS3*), SDY667 (*MAT his3Δ1, leu2Δ0, met15-Δ0, ura3 Δ0 ubx3Δ::URA3, END3-GFP::HIS3*), SDY668 (*MAT his3Δ1, leu2Δ0, met15-Δ0, ura3 Δ0 ubx3Δ::URA3, LAS17-GFP::HIS3*), SDY669 (*MAT his3Δ1, leu2Δ0, met15-Δ0, ura3 Δ0 ubx3Δ::URA3, MYO5-GFP::HIS3*), and SDY670 (*MAT his3Δ1, leu2Δ0, met15-Δ0, ura3 Δ0 ubx3Δ::URA3, ABP1-GFP::HIS3*). These strains were utilized for fluorescence microscopy in Figure 4A. SDY584 (*MAT*α *his3Δ1, leu2Δ0, met15-Δ0, ura3 Δ0*, *EDE1-RFP::KANMX4)* was mated with the Syp1-GFP strain from the GFP library (*MAT*a *his3Δ1, leu2Δ0, met15-Δ0, ura3 Δ0 SYP1-GFP::HIS*) to create diploid strain SDY595 (*MAT*a/*MAT*α *his3Δ1, leu2Δ0, met15-Δ0, ura3 Δ0 EDE1-RFP::KANMX4 SYP1-GFP::HIS*) which was subjected to sporulation and tetrad dissection, and resulting haploid segregant matted with SDY500. The resulting diploid strain was subjected to tetrad dissection to create SDY596 (*MAT his3Δ1, leu2Δ0, met15-Δ0, ura3 Δ0 ubx3Δ::URA3, EDE1-RFP::KANMX4, SYP1-GFP::HIS3).* SDY622 (*MATa ura3-52, his3Δ1, leu2Δ0, trp1-Δ901 EDE1-RFP::KANMX4, SLA1-*

GFP::TRP1) was mated with SDY500, sporulated and subjected to tetrad dissection to create SDY633 (*MAT*a *ura3-52, his3Δ1, leu2Δ0, trp1-Δ901 Δubx3::URA3*, *EDE1-RFP::KANMX4, SLA1-GFP::TRP1)*. Strain harboring a deletion of the UBX domain in the endogenous *UBX3* gene was created, SDY648 (*MATa his3Δ1, leu2Δ0, met15-Δ0, ura3 Δ0 EDE1-GFP::HIS3 ubx3$^{\Delta UBXd}$ ::URA3)*. Strains expressing Ubx1-7 –GFP from the endogenous locus were obtained from the GFP library.

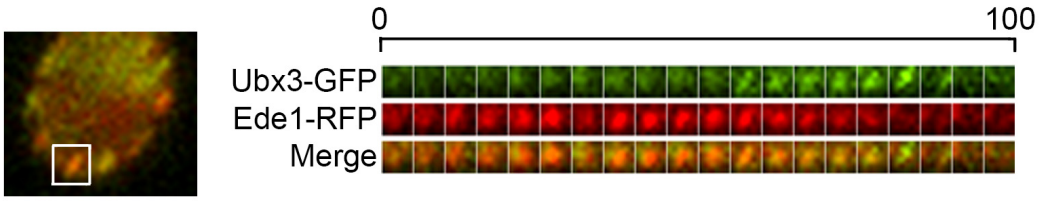

Figure S1. Ubx3 arrives to endocytic sites after early protein Ede1.
Dynamics of Ubx3-GFP and Ede1-RFP at endocytic sites were compared. Left, one frame of a movie indicating with a white box the endocytic site used for constructing a kymograph. Right, kymograph demonstrating dynamics of Ubx3-GFP and Ede1-RFP. Each frame = 5 sec.

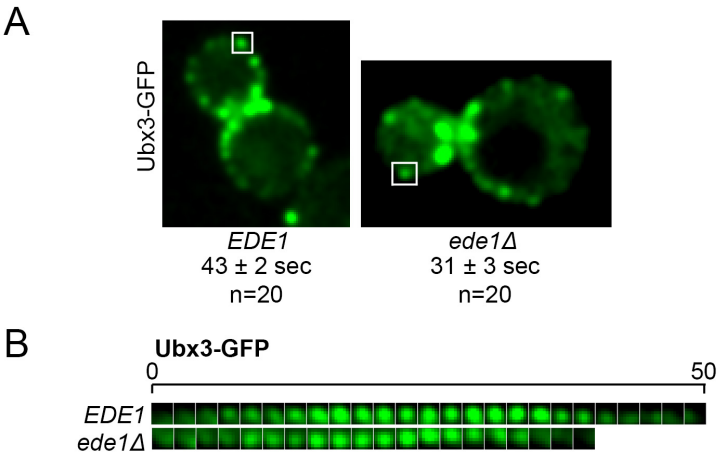

Figure S2. Ubx3 dynamics at sites of endocytosis depend on Ede1.
Ubx3-GFP has a decrease in endocytic patch lifetime in *ede1Δ* cells. Strains expressing Ubx3-GFP either in *EDE1* or *ede1Δ* background were analyzed by live cell fluorescence microscopy (20 patches per strain, $p<0.01$). Each frame = 2 sec.

Table S1: Proteins visualized in GFP screen

Screening Rank	Systematic Name	Common Name	PCC ± SD
1	YIR006C	PAN1	0.86 ± 0.01
2	YNL084C	END3	0.83 ± 0.06
3	YFR024C	YSC85	0.78 ± 0.06
4	YNL243W	SLA2	0.73 ± 0.11
5	YLR206W	ENT2	0.70 ± 0.04
6	YBL007C	SLA1	0.69 ± 0.09
7	YHR161C	YAP1801	0.65 ± 0.09
8	YJR005W	APL1	0.63 ± 0.18
9	YLR337C	VRP1	0.62 ± 0.39
10	YNR035C	ARC35	0.59 ± 0.07
11	YIL034C	CAP2	0.58 ± 0.11
12	YNL138W	SRV2	0.58 ± 0.09
13	YJL021C	BBC1	0.56 ± 0.04
14	YGL181W	GTS1	0.55 ± 0.12
15	YIL062C	ARC15	0.54 ± 0.07
16	YOR181W	LAS17	0.54 ± 0.05
17	YLR370C	ARC18	0.53 ± 0.13
18	YGR080W	TWF1	0.53 ± 0.11
19	YKL013C	ARC19	0.53 ± 0.05
20	YDL091C	Ubx3	0.52 ± 0.26
21	YIL095W	PRK1	0.51 ± 0.12
22	YPL221W	BOP1	0.50 ± 0.12
23	YDL012C		0.50 ± 0.14
24	YER071C	TDA2	0.49 ± 0.13
25	YKL007W	CAP1	0.48 ± 0.12
26	YCR088W	ABP1	0.48 ± 0.13
27	YMR109W	MYO5	0.47 ± 0.05
28	YOL062C	APM4	0.47 ± 0.15
29	YBL042C	FUI1	0.47 ± 0.02
30	YOR367W	SCP1	0.46 ± 0.10
31	YDL161W	ENT1	0.46 ± 0.31
32	YCR030C	SYP1	0.46 ± 0.01
33	YOR104W	PIN2	0.45 ± 0.19
34	YBL085W	BOI1	0.45 ± 0.05
35	YGR241C	YAP1802	0.45 ± 0.07
36	YGR026W		0.45 ± 0.03
37	YBL047C	EDE1	0.44 ± 0.19
38	YNL283C	WSC2	0.44 ± 0.07
39	YHR136C	SPL2	0.44 ± 0.18

40	YHR114W	BZZ1	0.43 ± 0.20
41	YCR009C	RVS161	0.43 ± 0.05
42	YBL029C-A		0.43 ± 0.12
43	YLR414C	PUN1	0.43 ± 0.04
44	YLL010C	PSR1	0.42 ± 0.07
45	YAL053W		0.42 ± 0.11
46	YGR281W	YOR1	0.42 ± 0.05
47	YBR016W		0.42 ± 0.05
48	YBR068C	BAP2	0.41 ± 0.06
49	YDR090C		0.41 ± 0.11
50	YDR034W-B		0.41 ± 0.09
51	YDR508C	GNP1	0.41 ± 0.15
52	YOL105C	WSC3	0.40 ± 0.05
53	YDR011W	SNQ2	0.40 ± 0.18
54	YGR065C	VHT1	0.40 ± 0.07
55	YOR094W	ARF3	0.40 ± 0.06
56	YER118C	SHO1	0.39 ± 0.16
57	YLR429W	CRN1	0.39 ± 0.19
58	YDR033W	MRH1	0.39 ± 0.15
59	YDR388W	RVS167	0.39 ± 0.12
60	YPR124W	CTR1	0.39 ± 0.07
61	YMR295C		0.38 ± 0.05
62	YML016C	PPZ1	0.38 ± 0.11
63	YOR165W	SEY1	0.38 ± 0.03
64	YMR266W	RSN1	0.38 ± 0.07
65	YPR171W	BSP1	0.38 ± 0.12
66	YML116W	ATR1	0.38 ± 0.07
67	YNL087W	TCB2	0.38 ± 0.04
68	YDR233C	RTN1	0.38 ± 0.05
69	YDR093W	DNF2	0.38 ± 0.02
70	YJR058C	APS2	0.38 ± 0.14
71	YDR344C		0.37 ± 0.05
72	YBR086C	IST2	0.37 ± 0.08
73	YDR210W		0.37 ± 0.05
74	YKR020W	VPS67	0.37 ± 0.25
75	YGL139W		0.37 ± 0.10
76	YDR039C	ENA2	0.36 ± 0.12
77	YML072C		0.36 ± 0.21
78	YDL240W	LRG1	0.35 ± 0.06
79	YLR332W	MID2	0.35 ± 0.07
80	YLR413W		0.35 ± 0.01

81	YBR052C		0.34 ± 0.08
82	YOR304C-A		0.34 ± 0.10
83	YDL189W	RBS1	0.34 ± 0.14
84	YKR100C		0.34 ± 0.08
85	YCR038C	BUD5	0.33 ± 0.09
86	YGL077C	HNM1	0.33 ± 0.12
87	YLR407W		0.33 ± 0.10
88	YLL028W	TPO1	0.33 ± 0.17
89	YNL020C	ARK1	0.33 ± 0.11
90	YIR003W	Aim21	0.33 ± 0.08
91	YGR191W	HIP1	0.33 ± 0.01
92	YOR043W	WHI2	0.32 ± 0.20
93	YDR384C	ATO3	0.32 ± 0.14
94	YDR038C	ENA5	0.32 ± 0.15
95	YOR273C	TPO4	0.32 ± 0.08
96	YER020W	GPA2	0.32 ± 0.07
97	YOR086C		0.32 ± 0.06
98	YMR212C	EFR3	0.32 ± 0.13
99	YNL106C	INP52	0.32 ± 0.09
100	YOL019W	TOS7	0.32 ± 0.08
101	YOR161C		0.32 ± 0.11
102	YHR107C	CDC12	0.31 ± 0.30
103	YPR149W	NCE102	0.31 ± 0.13
104	YER114C	BOI2	0.31 ± 0.03
105	YGL233W	SEC15	0.31 ± 0.12
106	YPL032C	SVL3	0.30 ± 0.05
107	YPL206C		0.30 ± 0.06
108	YIL147C	SLN1	0.30 ± 0.08
109	YPL214C	THI6	0.29 ± 0.11
110	YKL051W	SFK1	0.29 ± 0.18
111	YNR055C	HOL1	0.29 ± 0.09
112	YGR086C	PIL1	0.29 ± 0.10
113	YML028W	TSA1	0.29 ± 0.03
114	YDR040C	ENA1	0.29 ± 0.19
115	YBR069C	TAT1	0.29 ± 0.12
116	YLR166C	SEC10	0.29 ± 0.14
117	YIL121W	QDR2	0.29 ± 0.05
118	YLR319C	BUD6	0.29 ± 0.05
119	YDR479C	PEX29	0.28 ± 0.06
120	YPL058C	PDR12	0.28 ± 0.08
121	YFL034C-B	MOB2	0.28 ± 0.16

122	YIL068C	SEC6	0.28 ± 0.04
123	YPL265W	DIP5	0.28 ± 0.04
124	YEL060C	PRB1	0.28 ± 0.25
125	YDR357C	CNL1	0.28 ± 0.08
126	YMR058W	FET3	0.28 ± 0.15
127	YNL173C	MDG1	0.28 ± 0.17
128	YGR198W		0.28 ± 0.06
129	YLR138W	NHA1	0.28 ± 0.11
130	YGL008C	PMA1	0.28 ± 0.12
131	YIL105C	LIT2	0.27 ± 0.15
132	YDR166C	SEC5	0.27 ± 0.27
133	YNL268W	LYP1	0.27 ± 0.05
134	YNL233W	BNI4	0.27 ± 0.16
135	YGL200C	EMP24	0.27 ± 0.07
136	YGR121C	MEP1	0.27 ± 0.19
137	YGL108C		0.27 ± 0.19
138	YIL009W	FAA3	0.27 ± 0.13
139	YDL099W		0.26 ± 0.15
140	YBR234C	ARC40	0.26 ± 0.07
141	YOL020W	TAT2	0.26 ± 0.19
142	YBR102C	EXO84	0.26 ± 0.05
143	YDR170W-A		0.26 ± 0.05
144	YDR345C	HXT3	0.26 ± 0.03
145	YJL186W	MNN5	0.26 ± 0.13
146	YNL078W	NIS1	0.26 ± 0.11
147	YOR153W	PDR5	0.26 ± 0.05
148	YDR032C	PST2	0.25 ± 0.08
149	YCL024W	KCC4	0.25 ± 0.08
150	YFR024C-A	LSB3	0.25 ± 0.18
151	YBR043C	AQR2	0.25 ± 0.12
152	YOR070C	GYP1	0.25 ± 0.03
153	YGR130C		0.25 ± 0.06
154	YER133W	GLC7	0.24 ± 0.07
155	YDR348C	PAL1	0.24 ± 0.11
156	YHR146W	CRP1	0.24 ± 0.11
157	YPR066W	UBA3	0.24 ± 0.12
158	YKL129C	MYO3	0.24 ± 0.04
159	YLR353W	BUD8	0.24 ± 0.11
160	YGR138C	TPO2	0.24 ± 0.06
161	YJR076C	CDC11	0.24 ± 0.09
162	YOR233W	KIN4	0.24 ± 0.03

163	YMR092C	AIP1	0.24 ± 0.13
164	YOR042W	CUE5	0.24 ± 0.09
165	YDR343C	HXT6	0.24 ± 0.16
166	YEL017C-A	PMP2	0.24 ± 0.05
167	YOL084W	PHM7	0.24 ± 0.22
168	YOL047C		0.23 ± 0.17
169	YIL140W	AXL2	0.23 ± 0.05
170	YKR003W	OSH6	0.23 ± 0.05
171	YBL037W	APL3	0.23 ± 0.05
172	YAL055W	PEX22	0.23 ± 0.09
173	YER008C	SEC3	0.23 ± 0.14
174	YLL043W	FPS1	0.22 ± 0.07
175	YOL070C		0.22 ± 0.11
176	YBR109C	CMD1	0.22 ± 0.05
177	YCR004C	YCP4	0.22 ± 0.17
178	YEL063C	CAN1	0.22 ± 0.15
179	YKR093W	PTR2	0.22 ± 0.06
180	YGR255C	COQ6	0.22 ± 0.11
181	YLR237W	THI7	0.22 ± 0.01
182	YCL040W	GLK1	0.22 ± 0.09
183	YBR059C	AKL1	0.22 ± 0.11
184	YNL190W		0.22 ± 0.06
185	YHR123W	EPT1	0.21 ± 0.11
186	YLR084C	RAX2	0.21 ± 0.06
187	YLR423C	APG17	0.21 ± 0.08
188	YER145C	FTR1	0.21 ± 0.04
189	YGL156W	AMS1	0.21 ± 0.16
190	YNL085W	MKT1	0.21 ± 0.04
191	YDR373W	FRQ1	0.21 ± 0.11
192	YER054C	GIP2	0.21 ± 0.02
193	YPR138C	MEP3	0.20 ± 0.02
194	YBR255W		0.20 ± 0.12
195	YDR084C	TVP23	0.20 ± 0.02
196	YOR216C	RUD3	0.20 ± 0.10
197	YNL142W	MEP2	0.20 ± 0.05
198	YFR015C	GSY1	0.20 ± 0.09
199	YOL112W	MSB4	0.20 ± 0.04
200	YAL029C	MYO4	0.19 ± 0.02
201	YBR200W	BEM1	0.19 ± 0.21
202	YMR031C		0.19 ± 0.04
203	YCR002C	CDC10	0.19 ± 0.22

204	YPR049C	CVT9	0.19 ± 0.08
205	YPR156C	TPO3	0.19 ± 0.09
206	YHR004C	NEM1	0.19 ± 0.14
207	YDR022C	CIS1	0.19 ± 0.04
208	YOR326W	MYO2	0.18 ± 0.10
209	YDL146W		0.18 ± 0.15
210	YMR299C		0.18 ± 0.15
211	YDL225W	SHS1	0.18 ± 0.07
212	YPL249C	GYP5	0.18 ± 0.11
213	YMR011W	HXT2	0.18 ± 0.07
214	YLR258W	GSY2	0.18 ± 0.05
215	YBR008C	FLR1	0.18 ± 0.04
216	YHR147C	MRPL6	0.18 ± 0.07
217	YOL149W	DCP1	0.17 ± 0.09
218	YJL178C	ETF1	0.17 ± 0.10
219	YPL010W	RET3	0.17 ± 0.05
220	YNL238W	KEX2	0.17 ± 0.05
221	YML052W	SUR7	0.17 ± 0.16
222	YBL086C		0.17 ± 0.06
223	YDL019C	OSH2	0.16 ± 0.06
224	YDR497C	ITR1	0.16 ± 0.07
225	YGL203C	KEX1	0.16 ± 0.18
226	YKL103C	LAP4	0.16 ± 0.07
227	YDL058W	USO1	0.16 ± 0.01
228	YBR054W	YRO2	0.16 ± 0.10
229	YPR122W	AXL1	0.16 ± 0.01
230	YHL032C	GUT1	0.16 ± 0.11
231	YNL130C	CPT1	0.16 ± 0.04
232	YDL192W	ARF1	0.15 ± 0.18
233	YHR158C	KEL1	0.15 ± 0.09
234	YNL006W	LST8	0.15 ± 0.14
235	YGR166W	KRE11	0.15 ± 0.06
236	YNL194C		0.15 ± 0.12
237	YFL036W	RPO41	0.15 ± 0.03
238	YOR115C	TRS33	0.15 ± 0.08
239	YPL065W	VPS28	0.15 ± 0.08
240	YOL044W	PEX15	0.15 ± 0.03
241	YBR288C	APM3	0.15 ± 0.18
242	YKR001C	VPS1	0.15 ± 0.13
243	YMR319C	FET4	0.15 ± 0.16
244	YKL140W	TGL1	0.15 ± 0.08

245	YLR067C	PET309	0.14 ± 0.06
246	YDL222C		0.14 ± 0.08
247	YJR086W	STE18	0.14 ± 0.04
248	YCR024C-A	PMP1	0.14 ± 0.16
249	YKL041W	VPS24	0.14 ± 0.07
250	YPL004C	LSP1	0.14 ± 0.04
251	YIL045W	PIG2	0.14 ± 0.01
252	YMR010W		0.14 ± 0.13
253	YGR229C	SMI1	0.14 ± 0.08
254	YPL166W		0.14 ± 0.17
255	YEL015W	EDC3	0.13 ± 0.03
256	YMR163C		0.13 ± 0.01
257	YDR141C	DOP1	0.13 ± 0.05
258	YML085C	TUB1	0.13 ± 0.03
259	YML064C	TEM1	0.13 ± 0.11
260	YAR009C		0.13 ± 0.06
261	YLR035C-A		0.12 ± 0.04
262	YMR086W		0.12 ± 0.07
263	YJL024C	APS3	0.12 ± 0.15
264	YLR072W		0.12 ± 0.03
265	YLR291C	GCD7	0.12 ± 0.05
266	YNR056C	BIO5	0.12 ± 0.07
267	YLR187W		0.11 ± 0.07
268	YHR005C	GPA1	0.11 ± 0.05
269	YNL126W	SPC98	0.11 ± 0.08
270	YOL082W	CVT19	0.11 ± 0.02
271	YCR061W		0.11 ± 0.08
272	YLR250W	SSP120	0.11 ± 0.06
273	YMR183C	SSO2	0.11 ± 0.04
274	YHR011W	DIA4	0.10 ± 0.07
275	YEL005C	VAB2	0.10 ± 0.09
276	YMR253C		0.10 ± 0.09
277	YPR148C		0.10 ± 0.10
278	YNL065W	AQR1	0.10 ± 0.05
279	YMR080C	NAM7	0.10 ± 0.07
280	YOR109W	INP53	0.09 ± 0.02
281	YDR150W	NUM1	0.09 ± 0.00
282	YEL011W	GLC3	0.09 ± 0.14
283	YLR347C	KAP95	0.09 ± 0.04
284	YDR367W		0.09 ± 0.07
285	YNR016C	ACC1	0.09 ± 0.02

286	YLR219W	MSC3	0.08 ± 0.12
287	YLL001W	DNM1	0.08 ± 0.09
288	YDR484W	SAC2	0.08 ± 0.03
289	YFL047W	RGD2	0.08 ± 0.11
290	YBL017C	PEP1	0.08 ± 0.18
291	YCL001W	RER1	0.08 ± 0.06
292	YLL006W	MMM1	0.08 ± 0.07
293	YGL219C	MDM34	0.08 ± 0.04
294	YAR044W	OSH1	0.08 ± 0.11
295	YDR517W	GRH1	0.08 ± 0.09
296	YBR164C	ARL1	0.08 ± 0.07
297	YJL029C	VPS53	0.07 ± 0.08
298	YCL056C		0.07 ± 0.02
299	YOR127W	RGA1	0.07 ± 0.07
300	YHR182W		0.07 ± 0.06
301	YPR029C	APL4	0.07 ± 0.04
302	YNL297C	MON2	0.07 ± 0.06
303	YNL118C	DCP2	0.06 ± 0.03
304	YML071C	COG8	0.06 ± 0.08
305	YDR027C	LUV1	0.06 ± 0.09
306	YGL180W	APG1	0.05 ± 0.04
307	YMR124W		0.05 ± 0.04
308	YKR088C	TVP38	0.05 ± 0.11
309	YGR261C	APL6	0.05 ± 0.05
310	YDR270W	CCC2	0.04 ± 0.06
311	YDR222W		0.04 ± 0.09
312	YMR313C	TGL3	0.04 ± 0.02
313	YDR525W-A	SNA2	0.04 ± 0.12
314	YDR495C	VPS3	0.04 ± 0.03
315	YKL092C	BUD2	0.03 ± 0.01
316	YGL225W	VRG4 3	0.02 ± 0.04
317	YOR284W	HUA2	0.01 ± 0.05
318	YDL029W	ARP2	-0.01 ± 0.09
319	YDR129C	SAC6	-0.02 ± 0.03

Table S2: Endocytic proteins visualized in the GFP screen

Screening Rank	Systematic Name	Common Name	PCC ± SD
1	YIR006C	PAN1	0.863 ± 0.01
2	YNL084C	END3	0.825 ± 0.06
3	YFR024C	YSC85	0.779 ± 0.06
4	YNL243W	SLA2	0.727 ± 0.11
5	YLR206W	ENT2	0.704 ± 0.04
6	YBL007C	SLA1	0.695 ± 0.09
7	YHR161C	YAP1801	0.646 ± 0.09
8	YJR005W	APL1	0.626 ± 0.18
9	YLR337C	VRP1	0.615 ± 0.39
10	YNR035C	ARC35	0.594 ± 0.07
11	YIL034C	CAP2	0.584 ± 0.11
13	YJL021C	BBC1	0.559 ± 0.04
14	YGL181W	GTS1	0.547 ± 0.12
15	YIL062C	ARC15	0.539 ± 0.07
16	YOR181W	LAS17	0.536 ± 0.05
17	YLR370C	ARC18	0.529 ± 0.13
18	YGR080W	TWF1	0.527 ± 0.11
19	YKL013C	ARC19	0.526 ± 0.05
21	YIL095W	PRK1	0.505 ± 0.12
25	YKL007W	CAP1	0.482 ± 0.12
26	YCR088W	ABP1	0.481 ± 0.13
27	YMR109W	MYO5	0.473 ± 0.05
28	YOL062C	APM4	0.473 ± 0.15
30	YOR367W	SCP1	0.463 ± 0.10
31	YDL161W	ENT1	0.460 ± 0.31
32	YCR030C	SYP1	0.456 ± 0.01
35	YGR241C	YAP1802	0.451 ± 0.07
37	YBL047C	EDE1	0.445 ± 0.19
40	YHR114W	BZZ1	0.434 ± 0.20
41	YCR009C	RVS161	0.430 ± 0.05
57	YLR429W	CRN1	0.388 ± 0.19
59	YDR388W	RVS167	0.386 ± 0.12
65	YPR171W	BSP1	0.381 ± 0.12
70	YJR058C	APS2	0.375 ± 0.14
89	YNL020C	ARK1	0.328 ± 0.11
90	YIR003W	AIM21	0.327 ± 0.08
99	YNL106C	INP52	0.318 ± 0.09
140	YBR234C	ARC40	0.262 ± 0.07
155	YDR348C	PAL1	0.244 ± 0.11

158	YKL129C	MYO3	0.242 ± 0.04
171	YBL037W	APL3	0.227 ± 0.05
183	YBR059C	AKL1	0.216 ± 0.11
318	YDL029W	ARP2	-0.005 ± 0.09
319	YDR129C	SAC6	-0.016 ± 0.03